JOINT EUROPEAN TORUS

JET–P(92)02

S. Putvinskii
and JET Team

# Geometry of Drift Surfaces Near Magnetic Separatrix in a Tokamak with Poloidal Divertor

# Geometry of Drift Surfaces Near Magnetic Separatrix in a Tokamak with Poloidal Divertor

S Putvinskii
and JET Team*

***JET-Joint Undertaking, Culham Science Centre, OX14 3DB, Abingdon, UK***

** See Annex*

Preprint of Paper to be submitted for publication in
Plasma Physics and Controlled Fusion

# Geometry of Drift Surfaces Near Magnetic Separatrix in a Tokamak with Poloidal Divertor

S Putvinskii

JET Joint Undertaking, Abingdon, Oxon. OX14 3EA, UK

## Abstract

High energy particle drift orbits near the magnetic separatrix have been studied in order to analyze the divertor target plate heat load by the superthermal ions. It was found that the particle flux profile usually has three maximums at the toroidal drift facing divertor plate, and two at the opposite one.

It is shown that toroidal field ripple due to discreteness of the toroidal coils produces a ripple well region near the divertor X-point and as a consequence can change the distribution of the escaping particles over the target plates. The convective flux of the ripple trapped particles provides noticeable toroidal asymmetry of the particle flux profile, even at a very small ripple value of $\leq 10^{-3}$.

JET parameters have been considered as an example, but the results obtained are applicable to a tokamak-reactor as well.

## 1. Introduction

In tokamaks with poloidal divertor, the thermal heat flux from the plasma is concentrated in a thin layer near striking points at the divertor target plates. The bigger the tokamak, and the larger the thermal flux from the plasma, the smaller the relative thickness of the thermal scrape-off layer. This conclusion follows from 2D modelling of energy balance in the scrape-off layer, based on the transport equations [1]. In this approximation, the thickness of the layer is defined by the balance of thermal heat conductions along the field lines and across the layer. A prediction for tokamak reactors like ITER [2] with total fusion power of about 1 GW, indicates a very small thermal scrape-off layer thickness of about $\Delta_{sol} \cong 1$ cm. For such a narrow layer, there are a number of effects which give rise to a spreading of the particle and heat fluxes at the divertor plates.

One of them, the particle toroidal drift, has been used in [3-5] for interpretation of experimental observations of the divertor plate heat load patterns in JET. Because of the $\nabla B \times B$ drift particle orbits in a tokamak deviate from magnetic surfaces by a distance of $\Delta_{dr} \cong q\rho_L$ for transit and $\Delta_{dr} \cong q\rho_L/\epsilon^{1/2}$ for banana particles. Here $\rho_L$ is the particle Larmor radius, q the safety factor and $\epsilon$ the inverse aspect ratio. For particles with energy above several tens keV, $\Delta_{dp} > \Delta_{sol}$ and for the calculation of the high energy particle contribution to the divertor heat load, it is necessary to consider not magnetic, but drift surfaces. As the magnetic surfaces the drift surfaces have a separatrix which separates in the divertor configuration confined particle orbits from orbits intersecting the divertor plates. While there is only one magnetic separatrix, particles with different energies and pitch angles have different drift surface separatrixes and this leads to a spreading of particle heat load at the target plates. This effect is important, especially for the loss of high energy particles such as fusion alpha-particles in a tokamak reactor, or superthermal ions produced during neutral beam heating in tokamaks. The reason why the high energy particles are lost is not discussed in the present paper, but there is experimental evidence [6] that superthermal ions can be lost during bursts of MHD activity. Monte Carlo orbit following models show [7] that the loss of high energy ions may be caused by toroidal field ripple or MHD modes [8]. In any case, the divertor plate heat loads by high energy particles depends on the geometry of the drift surfaces near the divertor separatrix which are studied in section 2 of the present paper.

The second effect which can be important for the redistribution of the fast ion flux is toroidal field ripple (section 3). A ripple well region always exists in the vicinity of the magnetic X-point. The closer a magnetic field line is to the separatrix, the smaller $B\nabla|B|$ is, and therefore, an arbitrary small ripple produces magnetic wells near the X-point. It will be shown that in JET with 32 toroidal field coils and a very low ripple value, the width of the ripple well region is of the order 10 cm. Banana particles with their turning point in the ripple well region can be trapped and then drift vertically towards the target plate on the ion drift side. This effect does not change the ion confinement in the bulk plasma, but leads to a redistribution of ion flux over the divertor target plates. It is shown that the ripple trapping spreads the particle flux profile in the poloidal direction and also produces a peaked toroidal flux profile. The toroidal flux profile is analysed in section 4.

## 2. Axisymmetrical Magnetic Field

The drift surfaces of charge particles in the axisymmetrical field are defined by three constants of motion: particle energy, magnetic moment $\mu$, and angular momentum $P_\varphi$:

$$P_\varphi = mv_\parallel R + \frac{e\Psi}{2\pi c} \tag{1}$$

$$\mu = \frac{mv_\perp^2}{2B} \tag{2}$$

Here

$$\Psi = \Psi(R,Z) \tag{3}$$

poloidal flux, $B \cong B_\varphi \cong B_O R_O/R$ is the toroidal magnetic field, $B_O = B_\varphi/(R=R_O)$. The poloidal flux is defined to be zero at the magnetic axis. For the particular class of high energy particles to be considered here, the electric field will be neglected, and then:

$$v^2 = v_\parallel^2 + v_\perp^2 = const. \tag{4}$$

Combining Eqs. (1,2,3) one can easily obtain the equation describing the drift surfaces:

$$R^2 - RR_b - \left(\frac{e}{2\pi mcv}(\Psi - \Psi_b)\right)^2 = 0, \tag{5}$$

where $R_b$ and $\Psi_b$ are the two constants defining the drift surface. For banana particles they are actually the position of the particle turning point.

To study the geometry of drift orbits near the separatrix, it is more convenient to use 3D space, R,Z,$\Psi$ instead of the traditional R,Z plane [9]. In this space the drift surface may be represented as the intersection of the cylindrical surface Eq. (5) and surface Eq. (3), Fig. 1. To obtain the drift surface shape in the R,Z plane, it is necessary to project the three-dimensional curve (thick line) shown in Fig. 1, upon the R,Z plane. Here we shall use another projection of orbits, namely R,$\psi$ variables. A particular example is shown in Fig. 2, where the plasma boundary, first wall position and trajectory are shown in the configuration space and variables R,$\Psi$. The equilibrium $\Psi$(R,Z) corresponds to the JET X-point discharge (# 23083). One can change the drift orbit by changing the banana tip position. When the banana tip position is located out of the plasma region in R,$\psi$ space, the single banana trajectory splits into two transit particle orbits with the same value of $R_b$ and $\Psi_b$.

In order to avoid the prompt particle loss to the wall, we assume that there are no limiters located close to the plasma near the equatorial plane. In this case, particles may escape from the plasma only on the divertor target plates. Particle scattering and/or spatial diffusion leads to a random walk of the banana tip position. In the banana diffusion regime where $\tau_{dif}$ is greater than the particle bounce time $\tau_b$ this process may be considered as random displacement of the surface Eq. (5) marked as number 2 in Fig. 1. It can be seen from Fig. 1 and Fig. 2b that particles can reach the target plates by passing through one of the separatrix trajectories which have their X-points located on the curve given by

$$\frac{\partial \Psi(R,Z)}{\partial Z} = 0. \tag{6}$$

The curve Eq. (6) is represented by the dashed-dotted line in Fig. 1. Two separatrix drift surfaces for banana and transit particles are shown in Fig. 3 and Fig. 4.

The drift trajectory through the drift X-point goes strictly in the toroidal direction because the toroidal drift in this point is compensated by the vertical component of particle longitudinal velocity. Therefore, the particle at the separatrix has an infinite bounce time $\tau_b \to \infty$. In an actual machine, small magnetic (and electric) field perturbations destroy the drift surfaces near the separatrix, and produce an ergodic layer similar to the ergodic layer in the vicinity of the magnetic separatrix.

The position of the X-point on the line Eq. (6) depends on the particle energy, and pitch angle. In order to calculate the splitting at the X-point position, the following dimensionless variables are introduced:

$$x = (R - R_x)/a, \quad z = (Z - Z_x)/a, \quad \psi = (\Psi - \Psi_x)/2\pi a^2 B_\varphi(R_x).$$

In these variables, Eq. (5) takes the form:

$$\Phi(x,z) = \frac{\rho_L^2}{\bar{\varepsilon}}(x - x_b)(1 + \varepsilon x) - (\psi - \psi_b)^2 = 0 \tag{7}$$

where a is the plasma minor radius, $\varepsilon = a/R_X$, $\rho_L = \rho_L/a$, $\rho_L$ is the particle Larmor radius. Using the closeness of the drift X-point to the magnetic X-point, $x < \varepsilon$, it is convenient to expand $\psi(x,z)$ in a series near the saddle point. To leading order we have

$$\psi \equiv k\left\{\frac{x^2 - z^2}{2}\sin(2\alpha) - xz\cos(2\alpha)\right\}, \tag{8}$$

where here $\alpha$ is the angle between the separatrix magnetic line, and the equatorial plane, and k is a dimensionless parameter $\approx 1/q_{0.95}$.

The drift X-point is a saddle point of the surface Eq. (7) and its coordinates are obtained from the equations $\partial\Phi/\partial x = 0$, $\partial\Phi/\partial z = 0$. These equations are

$$z = -x\, ctg(2\alpha), \tag{9}$$

and

$$\frac{kx(\psi - \psi_b)}{\sin(2\alpha)} = \frac{\rho_L^2}{2\varepsilon}(1 + 2\varepsilon x - \varepsilon x_b). \tag{10}$$

Eliminating $\psi_b$, $\psi$ and z from Eqs. (7-10) one obtains the following equation for the x coordinate of drift surface X-point:

$$\frac{x^2(x - x_b)(1 + \varepsilon x)}{(1 + 2\varepsilon x - \varepsilon x_b)^2} = M, \tag{11}$$

where

$$M = \frac{\rho_L^2 \sin^2(2\alpha)}{4\varepsilon k^2}.$$

In the dimensional variables

$$M = \left.\frac{\pi^2 \rho_L^2 R_x B_o^2}{a^3\left(\partial^2\psi/\partial R^2\right)^2}\right|_{R=R_x, Z=Z_x}.$$

In the zero banana width limit, Eq. (11) gives the solution

$$x = \begin{cases} 0 & x_b < 0, \\ x_b & x_b > 0. \end{cases}$$

The finite banana width effect can be estimated analytically for particular values of $x_b$. We obtain:

$$x = \begin{cases} \pm 2(M\varepsilon)^{1/2} & x_b = -1/\varepsilon \quad (v_\parallel = \pm v), \\ M^{1/3} & x_b = 0 \quad , \\ x_b + M/x_b & x_b >> M^{1/3} \quad . \end{cases} \tag{12}$$

Fig. 5 shows the dependence $x = x(x_b)$ obtained from the solution of Eq. (11) for the JET equilibrium used above, and three particular values of M, which correspond to tritons with

energies E = 10, 100, 1000 keV. The banana particle with the same major radius at the tip, as the magnetic X-point, have maximum shift of the drift X-point from the magnetic X-point.

The topology of separatrix surfaces of two transit particles and the banana particle are shown qualitatively in Fig. 6. The separatrixes for banana and transit particles with $v_{||} > 0$ are shifted to the right hand side of the magnetic separatrix but the transit particles with $v_{||} < 0$ shift to the torus axis. The direction of particle motion along the separatrixes is shown in Fig. 6 by arrows. It can be seen that the particle striking points are located between magnetic separatrix striking points at the target plate in the ion drift side and outside the magnetic separatrix striking points at the opposite target plate.

The position of the particle striking point at the target plate depends on the magnetic field geometry and the target plate configuration, but the general features may be obtained by analysing the following simplified model. We consider straight horizontal plates located at a small distance $z_w \lesssim \varepsilon$ from the magnetic X-point.. Using the approximation Eq. (8) for the poloidal magnetic field, Eq. (7), and with the above solutions $x = x(x_b)$, one can easily calculate the position of striking points 1-3, and 1'-3' (Fig. 6), as functions of particle pitch angle (or $x_b$). Figs. 7 and 8 show the dependence of radial coordinates of the particle striking points $x_w$ as functions of $x_b$ calculated for low (E = 10 keV) and high (E = 1 MeV) energy particles and the JET equilibrium.

At the low energy there is an inaccessable or "dead" zone at the toroidal drift facing side (between points a and b in Fig. 7). As the particle pitch angle decreases ($x_b$ increase) and the transit particle with $v_{||} > 0$ is becoming the banana particle, the striking point position (marked by 3 in Fig. 7) jumps radially from point a to point b in Fig. 7 and then continues to change its position in accordance with curve 2.

For the high energy particle with large banana width, there is no "forbidden" zone and the striking point position changes gradually with pitch angle Fig. 8.

In order to calculate the particle flux profile over the target plates due to the drift effects, the dependence of particle flux on particle pitch angle or $\Phi(x_b)$ must be known, and this requires a detailed knowledge of the diffusion rate at the plasma periphery. Here it is convenient to assume $\Phi(x_b) = \text{const}$. The particle flux density is then proportional to $dx_b/dx_w$ which can be calculated directly from the dependencies presented in Figs. 7 and 8. The particle flux profiles are shown in

Figs. 9 and 10. It can be seen that the distribution, especially at the low energy, consists of very narrow peaks from transit particles (1', 3, 1, 2', 3') and more broad distribution of banana particles (2). The shift of the transit particle peak from the magnetic separatrix striking point can easily be obtained from Eqs. (7) and (12) by putting $x_b = -1/\varepsilon$:

$$\Delta x_w = x_w - x_s = \pm\frac{(M\varepsilon)^{1/2}}{\sin^2(\alpha)} \quad \text{for outer striking point,}$$
$$\Delta x_w = x_w - x_s = \pm\frac{(M\varepsilon)^{1/2}}{\cos^2(\alpha)} \quad \text{for inner striking point.} \tag{13}$$

For example the peak displacement for fusion dd-tritons in JET is about $\Delta x_w \cong 0.36(E)^{1/2}$ cm, where E is the energy in MeV. The spreading of the narrow peak arises from averaging over the particle energy distribution function. For a wide distribution function, a half width is approximately equal to $\Delta x_w$.

For high energy particles the spreading of the particle flux profile due to drift, dominates over the spreading caused by particle transport across the magnetic surface . The spreading due to particle transport [10] can be estimated as

$$\Delta x_w^c \cong \left(D\tau_b\right)^{1/2}/a \approx 1/\nu \tag{14}$$

Comparing Eq. (13) and Eq. (14) one would obtain in JET $D \cong 10^4$ cm$^2$/s, $\Delta x_w^c < \Delta x_w$ for $E > 1$ keV.

For the double null (DN) magnetic configuration Fig. 6, the magnetic separatrix and the drift separatrices have two X-points. But, in the loss of up-down symmetry, particles can have single null drift separatrixes even in the DN magnetic configuration. In the symmetrical case the fluxes to the up and down plates should be almost equal. The difference between the up and down fluxes is determined by the radial profile of the particle diffusion rates. If the diffusion rate decreases with minor radius, then the particle load at the upper plate will be larger than at the down one as can be seen from Fig. 6, by comparing opposite sides of trajectories a-f. The asymmetry in the upper and lower plate particle loads $F_{up}$, $F_{down}$ can be estimated to be

$$\frac{F_{down} - F_{up}}{F_{down} + F_{up}} \cong \frac{\partial D}{\partial \rho}\Delta\rho_b,$$

and is large for high energy particles with large banana width $\Delta\rho_b$.

The limiters located near the equatorial plane can change the up-down symmetry, but only when the diffusion rate $D > \rho_L^2 q^2/\tau_b$ is large at the plasma periphery. In the latter case, the limiter will cut off the flux to the plate which is opposite to the toroidal drift direction side.

In the symmetrical DN, the configuration ratio of the plate load near the outer and inner striking points depends on poloidal inhomogeneity of the diffusion rate. If the particle diffusion rate is larger at the outer part of the plasma cross section, trajectories (c-f) in Fig. 6 than at the inner part, trajectories a,b then, the particle flux near the outer striking point will be larger than that near the inner one. One can change the partition of flux between the outer and inner striking zones by applying magnetic or electric field perturbations which are resonant with the outer (c-f) or inner (a,b) parts of the particle trajectories.

## 3. Ripple Loss Through the Divertor Scrape-Off Layer

The effect of the magnetic field ripple due to discreteness of the tokamak toroidal field coils on the plasma energy and particle confinement has received much attention and studies reported in the literature [11]. Previous work deals mainly with the bulk plasma and the region near the poloidal divertor X-points has received less attention. It will be shown here that the magnetic field ripple near the X-point can have a significant effect on the particle orbits and the distribution of the particle flux onto the divertor plates.

The rippled toroidal field can be described by the following standard expression [11]:

$$B_\varphi = B_o \frac{R_o}{R}(1+\delta(r,z)\cos N\varphi), \tag{15}$$

where N is the number of toroidal field coils. At the large ripple value, the magnetic field strength $|B| \cong B_\varphi$ may be non monotonic along the field line and in this case the ripple wells exist and the particle may be trapped between two toroidal field coils. However, the ripple value in tokamaks is typically, $\delta \cong 1\%$ and the ripple wells only exist in the outboard side of the plasma cross section. Neglecting small terms order of $\delta^2$ and $B_R/B_\varphi$ the boundary of the ripple well region can be described by the equation

$$b = \frac{B_R}{B_\varphi N\delta(r,z)} = 1. \tag{16}$$

Here, $B_R$ is a radial component of the poloidal field. In the ripple well region $b < 1$. Because $B_R = 0$ at the equatorial plane (up-down symmetric configuration) the ripple wells always exist near the equatorial plane. In a tokamak with a poloidal divertor; there is another line, where $B_R = 0$ which passes through the X-point. This is illustrated in Fig. 11, where the ripple well region boundary is shown for JET X-point equilibrium. Ripple wells exist outside of the boundary 1, Fig. 11.

The well depth, which has been calculated for a typical JET configuration, monotonically increases in the vertical direction, Fig. 12. This is an important point for further consideration.

A banana particle diffusing towards the drift separatrix can be trapped in a well and then lost from the plasma through toroidal drift. There are two proceses in which ripple well trapping can occur: the trapping due to Coulomb collisions with the background plasma [12]; and collisionless trapping due to finite banana width effects [13]. As was shown in [13], the collisionless trapping is the dominant trapping mechanism for superthermal particles with energy above several tens keV. Because of the final banana width, the particle approaching the turning point and on being reflected, moves into regions with increasing ripple values. In the well region near the X-points, the well depth increases in the vertical direction and therefore the trapping can only occur at the toroidal drift facing plasma side for particles with an unfavourable toroidal position at the turning point. The toroidal precession of the banana orbit, and consequently, the randomisation of the banana particle position in the toroidal direction suggests a probabilistic description for the trapping process. The probability of trapping during one reflection has been calculated in [13]

$$p \cong \frac{V_{dr}\lambda R_b}{2\pi N v b \delta^{1/2}} T(b) \tag{17}$$

where

$$\lambda = \frac{1}{\delta}\frac{\partial \delta}{\partial z}; \qquad T = \frac{16\left(2\left(1-b^2\right)\right)^{1/2}\cos^{-1}(b)}{\pi\left[\left(1-b^2\right)^{1/2} - b\cos^{-1}(b)\right]^{1/2}},$$

and $V_{dr}$ is the toroidal drift velocity. The last expression was obtained in the adiabatic approximation, when the timescale of the ripple variation along the trajectory

$$t_{rip} = \left( \frac{V_{dr}}{\delta} \frac{\partial \delta}{\partial z} \right)^{-1}$$

is larger than the bounce time of the ripple well trapped particle

$$\tau_b = \frac{2\pi R}{N v \delta^{1/2}},$$

and imposes an upper limit on the particle energy

$$\frac{\tau_b}{t_{rip}} \cong \frac{\rho_L}{a\delta^{1/2}} << 1.$$

The last inequality for the JET ripple profile, $\delta \cong 5 \cdot 10^{-4}$ gives the upper limit for the energy E ≅ 100 keV.

At the high particle energy $\rho_L/a >> \delta^{1/2}$, Eq. (17) is unvalid and a numerical calculation is required. Starting from the guiding centre equations of motion, which in the dimensionless variables used above can be written as follows:

$$\begin{aligned}
\dot{x} &= \chi \frac{\partial \psi}{\partial z}, \\
\dot{z} &= -\chi \frac{\partial \psi}{\partial x} + \rho_L \left( 1 - \frac{1 + \varepsilon x_b}{2(1 + \varepsilon x)} \right), \\
\dot{\varphi} &= \frac{\chi}{(1 + \varepsilon x)}, \\
\dot{\chi} &= \frac{(1 + \varepsilon x_b)}{2(1 + \varepsilon x)^2} \left\{ \varepsilon (1 + \delta \cos N\varphi) \frac{\partial \psi}{\partial z} + \delta N \sin N\varphi \right\}.
\end{aligned} \tag{18}$$

where $\chi = v_{||}/v$ and the normalised time is $\tau = tv/R_x$. The contribution of the ripple field in the first three equations have been discarded as unimportant [11].

We shall again consider the vicinity of the X-point, x, z < ε where Eqs. (18) can be further simplified. The particle trapping occurs during its motion in that well which is closest to the particle turning point $\varphi_b$, where $\varphi - \varphi_b < 2\pi/N$. The radial projection of the field line with the length of one well is equal to $\Delta r \cong 2\pi R_o B_R / N B_\varphi \cong 2\pi R_o \delta << a\varepsilon$ and the particle vertical displacement from the turning point can be estimated as follows:

$$\Delta z = V_{dr} \Delta t \cong V_{dr} \frac{R_o}{N v \delta^{1/2}} \cong \frac{\rho_L}{N \delta^{1/2}} << a\varepsilon.$$

The last condition imposes an upper limit on the particle energy $\rho_L/a\delta^{1/2} < N\varepsilon$ which for JET parameters is typically E < 1 MeV.

Omitting the small term $O(\varepsilon^2)$, $O(1/N)$ and $O(\delta^{1/2}\varepsilon/q)$, Eq. (18) can be simplified as follows

$$\begin{aligned} \dot{z} &= \rho_L/2, \\ \dot{\varphi} &= \chi, \\ \dot{\chi} &= \frac{1}{2}\left\{\varepsilon\frac{\partial\psi}{\partial z} + \delta N \sin N\varphi\right\} \end{aligned} \tag{19}$$

Near the X-point, $\partial\delta/\partial z >> \partial\delta/\partial x$, i.e. $\delta = \delta(z)$. At the small distance of $\Delta R, \Delta z \cong \varepsilon$ one can assume

$$\lambda = \frac{1}{\delta}\frac{\partial\delta}{\partial z} = const, \quad or \quad \delta = \delta(z_b)\exp\left[\lambda(z - z_b)\right]. \tag{20}$$

In comparison with the exponential dependence (20), the first term in the last equation (19) may be considered as constant, $\partial\psi/\partial z \cong \partial\psi(x_b, z_b)/\partial z$. Renormalising $\tau_1 = \tau(\delta(z_b)N^2/2)^{1/2}$ one can obtain

$$\frac{\partial^2\xi}{\partial\tau_1^2} = b + \exp(a\tau_1)\sin\xi, \tag{21}$$

where

$$a = \frac{\rho_L\lambda}{N(2\delta)^{1/2}}; \quad b = \frac{B_R}{NB_\varphi\delta(z_b)}.$$

By means of these two parameters, the analytical expression (17) can be rearranged as

$$p = \frac{a}{2\sqrt{2}\pi b}T(b). \tag{22}$$

The last equation is valid for $a << 1$. To obtain the trapping probability at $a \cong 1$, Eq. (21) has been solved numerically and the probability of the trapping is defined as a ratio of the phase volume of particles trapped in the well during one bounce to total phase volume. A good agreement with the analytic expression has only been found at very small values of $a < 0.1$. At JET, parameters $a = 0.1$ correspond to the particle energy of $E \cong 10$ keV. The probability contours in the a,b plane are shown in Fig. 13. For $a > 0.1$, where Eq. (22) is invalid, the probability p(a,b) calculated numerically can be approximated by the following function:

$$p(a,b) = \frac{a}{\left(0.12b^2 + a^2\right)^{1/2}}F(b - 1.8a) \tag{23}$$

where

$$F(x)=\begin{cases}1 & ; \quad x<-0.4 \\ (1-x)/1.4 & ; \quad -0.4<x<1 \\ 0 & ; \quad 1<x\end{cases}$$

The accuracy of this approximation is better than 10% for $0.1 < a < 1.5$ and $0.1 < b < 3$.

The position of the ripple well trapping region in JET configuration is shown in Fig. 14. The magnetic separatrix is marked by the dashed line and line $B_R = 0$ by a dotted-dashed line. Ripple wells exist above the line with the solid circles in Fig. 14. When the banana tip moves in the vertical direction, the probability of ripple well trapping changes from zero to unity, increasing rapidly, from 0 to 0.8 in the shadowed region of Fig. 14. It is seen that the shadowed regions corresponding to different particle energies are rather narrow (because of the finite banana width corrections, the boundary of the ripple well region is located below the line Eq. (16)). As the ripple well depth increases in the vertical direction, the particle which has become trapped will be lost to the divertor target plates.

Therefore, particles with energy above several tens keV have a well defined trapping region boundary given by

$$\frac{B_R}{NB_\varphi \delta(r_b, z_b)} = 1 + \frac{\rho_L \lambda}{N(2\delta)^{1/2}}, \tag{24}$$

above which a particle will be trapped in a magnetic well in a few bounce periods and lost to the target plate on the ion drift side through ripple trapping.

It is clear that there is a particle energy above which the banana width becomes larger than the distance between X-point and ripple trapping boundary. For JET, ripple trapping occurs for particle energy up to 1 MeV.

The lower limit on the particle energy given by

$$\frac{\rho_L}{a} < \frac{a\nu_i}{\upsilon\delta},$$

is defined by Coulomb collision, which expels the particle from a well before it reaches the wall by vertical drift. Here, $\nu_i$ is the scattering frequency. For JET parameters, the last equation is fulfilled for deuteron energy of $E \gtrsim 10$ keV.

## 4. Toroidal Distribution of Ripple Trapped Particle Flux

The ripple trapped particles are located between toroidal field coils and therefore provide toroidal asymmetry in the particle flux at the target plates. The poloidal profile is rather broad (poloidal width $\cong \epsilon a$) and is not linked to the magnetic separatrix striking points. The profile shape depends on the poloidal distribution of the banana particle fluxes from the plasma core and can be calculated on the basis of knowledge of the particle fluxes. In a general case and depending on the form of the rippled field it is possible to estimate the toroidal distribution of the flux.

Because the width of the grey zone where the trapping probability changes from zero to 0.8, $\Delta z \cong a/N$ is small in comparison to $\epsilon a$, the trapping process can be described by the following equation

$$0 = -p(z)\frac{n(z)}{\tau_b} + D\frac{\partial^2 n(z)}{\partial z^2}. \tag{25}$$

Here, n(z) is the banana particle density with the banana tip position at z, D is the particle diffusion rate across the trapping boundary, $z = z_0(x)$, and $\tau_b$ is the banana particle bounce time. The real dependence p(z) can be replaced by a simplified one

$$p(z) \cong \frac{1-b+1.8a}{1.4} \cong -\frac{\partial b}{\partial z}\frac{(z-z_o)}{1.4} \cong \frac{\lambda b(z-z_o)}{1.4},$$

and D will be considered to be constant within the narrow trapping zone. In the new variable

$$y = (z-z_o)\left(\frac{\lambda b}{1.4\tau_b D}\right)^{1/3},$$

Eq. (25) can be rewritten as

$$\frac{\partial^2 n}{\partial y^2} - y\,n = 0. \tag{26}$$

Eq. (26) describes the density of the banana tip positions near the boundary of the ripple trapping region $z = z_0$. The solution of Eq. (26) for the appropriate boundary conditions $n_{|z=z_0} = n_o$, $n_{|z\to\infty} = 0$ is

$$n = n_o y^{1/2}\frac{\Gamma(2/3)}{3^{1/3}}\left\{I_{-1/3}\left(\frac{2y^{3/2}}{3}\right) - I_{1/3}\left(\frac{2y^{3/2}}{3}\right)\right\}, \tag{27}$$

where $\Gamma(x)$ is the gamma function and I(x) is the modified Bessel function [14]. The number of banana particles f(y) trapped at y can be estimated as:

$$f(y) = p(y)\frac{n}{\tau_b} \cong y\, n(y). \tag{28}$$

The longitudinal distribution function of the particles oscillating along the field line in the ripple well

$$g(l) = \frac{dl}{\upsilon_{\|}(l)}, \tag{29}$$

can be evaluated by replacing the real magnetic field profile in the well by a parabolic one. Then,

$$g(\varphi)d\varphi = \frac{d\varphi}{\pi\left(\varphi_{\max}^2 - \varphi^2\right)^{1/2}}. \tag{30}$$

Here $\varphi$ is the toroidal angle with $\varphi = 0$ equidistant between the toroidal field coils. The amplitude of particle oscillations in the well, $\varphi_{max}$, depends on the position of particle trapping in the well, $\varphi_{max} = \varphi_{max}(y)$. It is easy to show that near the ripple well boundary, $\varphi_{max} = 3(1\text{-}b)^{1/2}/(\sqrt{2N})$, or with the finite Larmor radius corrections similar to (23):

$$\varphi_{\max} = \frac{3(1-b+1.8a)^{1/2}}{\sqrt{2}N} \cong 3\frac{\left(1.4\lambda^2 b^2 D\tau_b\right)^{1/6}}{\sqrt{2}N} y^{1/2} \equiv \varphi_o y^{1/2}. \tag{31}$$

Weighting (30) with (28) one can obtain

$$g(\varphi) = const\int \frac{f(y)\,dy}{\left(\varphi_{\max}^2 - \varphi^2\right)^{1/2}} = const \int_{\frac{\varphi^2}{\varphi_o^2}}^{\infty} \frac{f(y)\,dy}{\left(y-(\varphi/\varphi_o)^2\right)^{1/2}}. \tag{32}$$

Fig. 15 shows the toroidal distribution of particle flux evaluated by numerical integration in Eq. (32). The half width of the toroidal distribution is equal to $\varphi_0$ and because of the growth of the well depth, decreases during the particle drift motion from the trapping boundary to the target plates . The decrease of $\varphi_0$ can be estimated roughly from conservation of the longitudinal invariant of the ripple trapped particles, $J = \oint \upsilon\, d\ell$ = const. At the target plates, $\varphi_{ow}^2 \cong \varphi_o^2 (\delta_o/\delta_w)^{1/2}$ where $\delta_w$ is the ripple value at the target plate. For JET, $\varphi_0 = 0.15$, $\delta_w/\delta_0 = 10$, and the half width of the distribution will be about $\Delta\varphi/(2\pi/N) \cong 0.5$.

## Conclusions

The superthermal particle drift orbits close to the magnetic separatrix has been analysed. If there is only one magnetic separatrix, the particles with different pitch angles and energies have

different drift separatrixes with different positions of the X-point. The splitting of the X-point due to the drift effect is actually one dimensional. All drift X-points are located at the line $\partial\psi/\partial z = 0$. The shift of the drift X-point from the magnetic one was calculated analytically for the general case.

The toroidal field ripples due to discreteness of the toroidal field coils can change the toroidal distribution of escaping particles. It was shown that near the magnetic X-point, ripple wells always exist, which gives use to ripple trapping of the banana particles before they reach the drift separatrix. The fraction of high energy particles which are trapped in the ripple wells is estimated to be $\cong \varepsilon < 1$, but a significant toroidal peaking factor leads to noticeable target heat load.

The analysis in this paper is based on the simple model assumptions and in some areas requires a more detailed calculation, but the approach may be useful for understanding the result of Monte-Carlo orbit following modelling and in the interpretation of experimental results.


## Acknowledgement

The author would like to thank Drs. T. Stringer, B Tubbing, W G F Core, for helpful discussions, and P Bararbaschi for supplying JET ripple profile and equilibrium configurations.


## References


[1] P C Stangeby, G M McCracken, Nucl. Fusion **30**, 1990, 1225.

[2] "ITER Concept Definition", IAEA, Vienna, 1989.

[3] M A Kovanen, et al, JET-P(91)06.

[4] D D Summers, M Lesourd, R Reichle, J-P Schulz, Y Zhu, JET Papers to 18$^{th}$ EPS Conference on Controlled Fusion and Plasma Physics, JET-P(91)08.

[5] W G F Core, E Lazzaro, JET-R(91)01, 1991.

[6] G J Sadler et al., Fusion Tech. **18**, 1990, 556.

[7] K Tani, T Takizuka, M Azumi, ITER-IL-PH-1-9-J-1,2, 1989.

[8] S Konovalov, S Putvinskii, Fusion Tech.**18**, 1990, 397.

[9] S Putvinskii, Sov. J. Plasma Phys. **14**(10), 1988, 729.

[10] S Putvinskii, Sov. J. Plasma Phys. **15**(2), 1989, 73.

[11] P Yushmanov, Review of Plasma Theory, ed. by B B Kadomtsev, vol. 16, 1987.

[12] T E Stringer, Nucl. Fusion **12**, 1972, 689.

[13] R J Goldston, H H Towner, J. Plasma Phys. **26**, part 2, 1981, 283.

[14] M Abramowiz, I Stegun, Handbook of Mathematical Functions, Dover Publications Inc., New York.

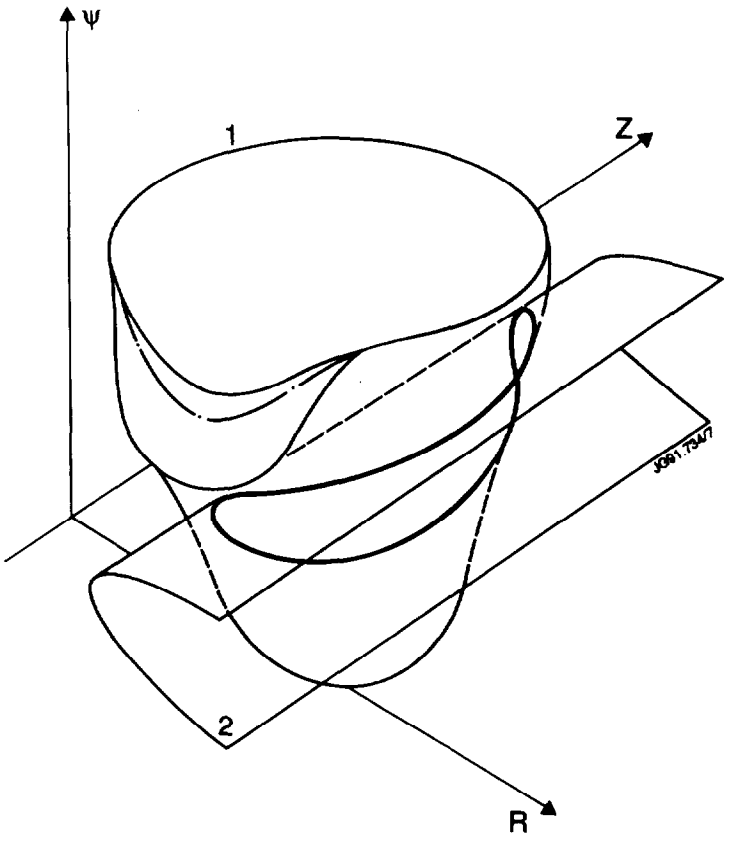


Fig. 1 The drift orbit (thick line) is the intersection of two surfaces in R,ψ,z space: 1) $\psi = \psi(R,Z)$, 2) cylindrical surface Eq. (5).
Dashed-dotted line shows $B_R = 0$.

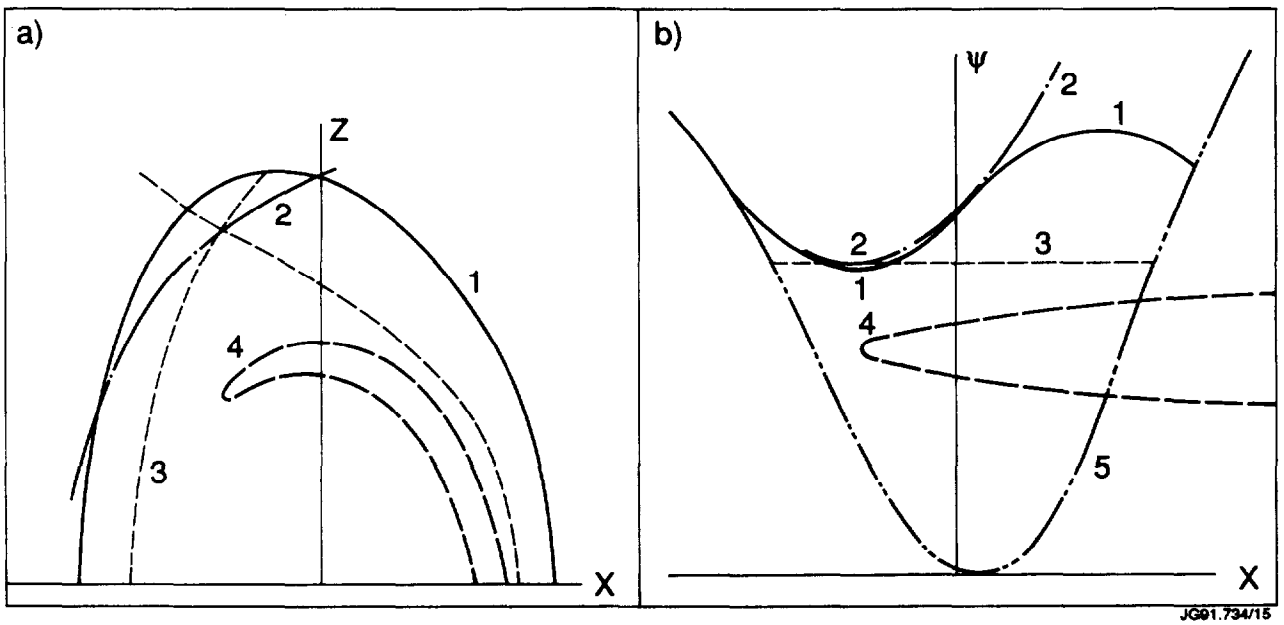


Fig. 2 Plasma boundary (3), banana particle trajectory (4), first wall (1) and line $B_R = 0$ (2) in R,Z variables (Fig. 2a) and x,ψ variables (Fig. 2b). JET double null configuration.

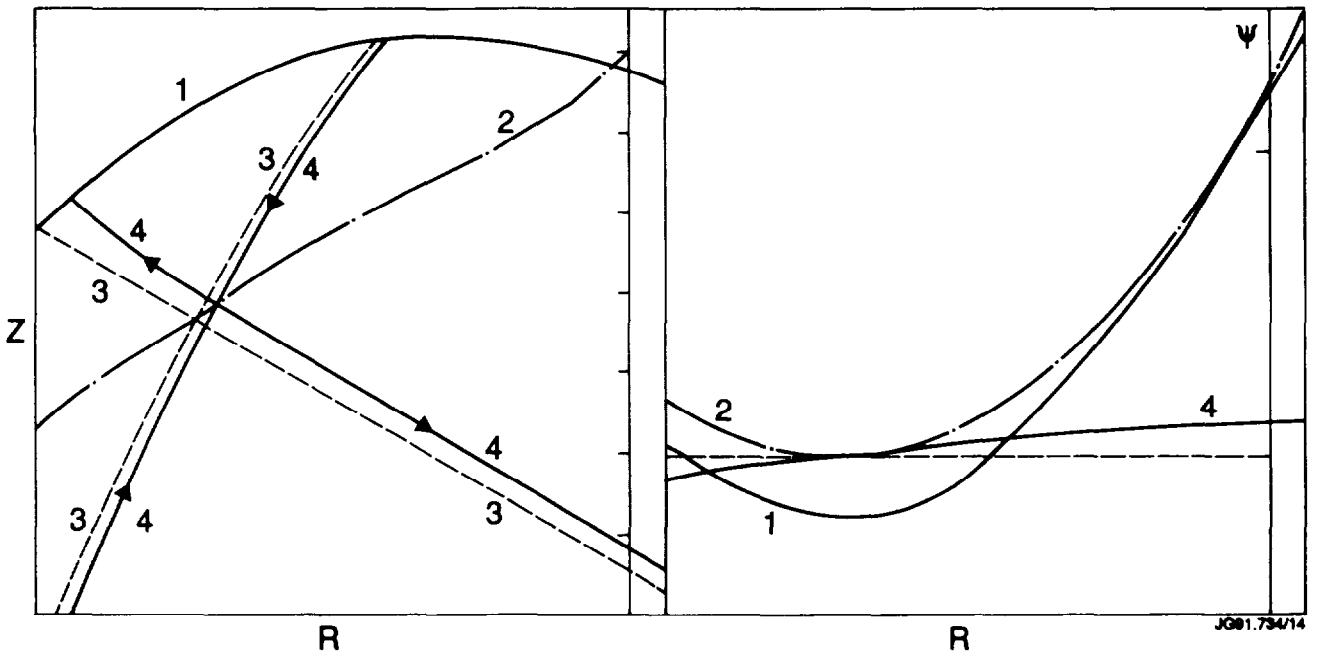


Fig. 3 A separatrix drift surface (4) for transit particle, E = 100 keV. Dashed line (3) shows magnetic separatrix. 1) first wall, 2) line $B_R = 0$.

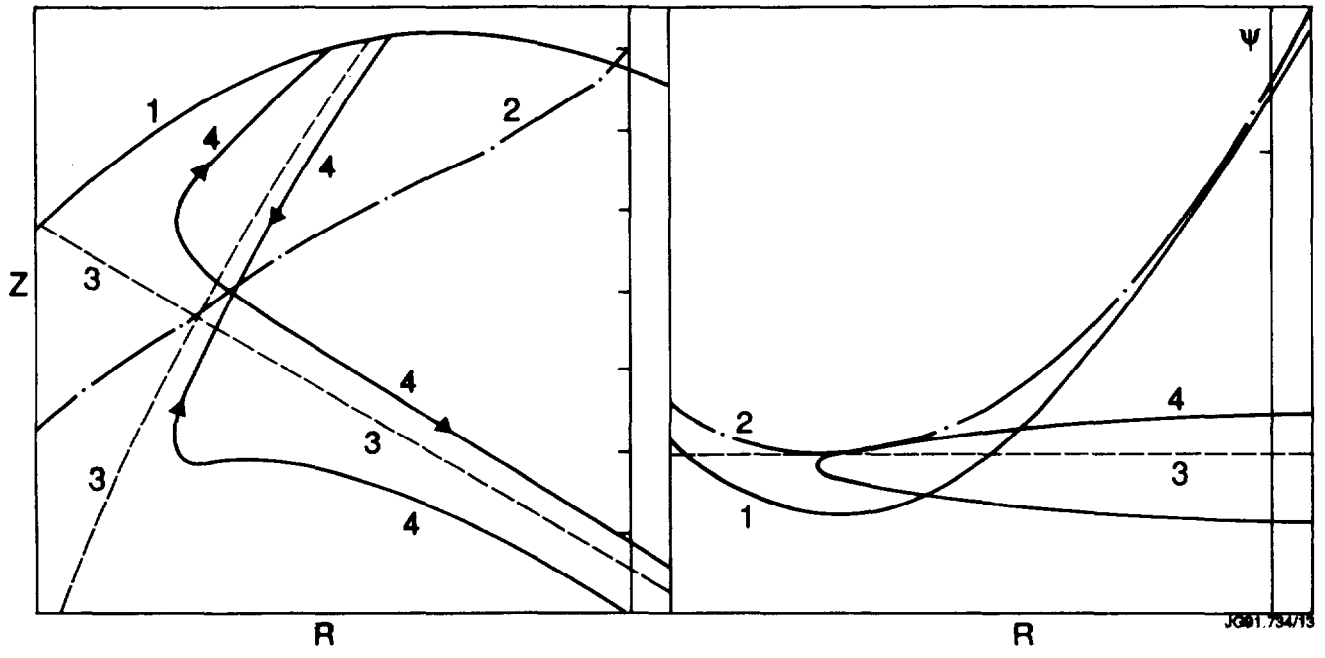


Fig. 4 The same as Fig. 3, but for the banana particle.

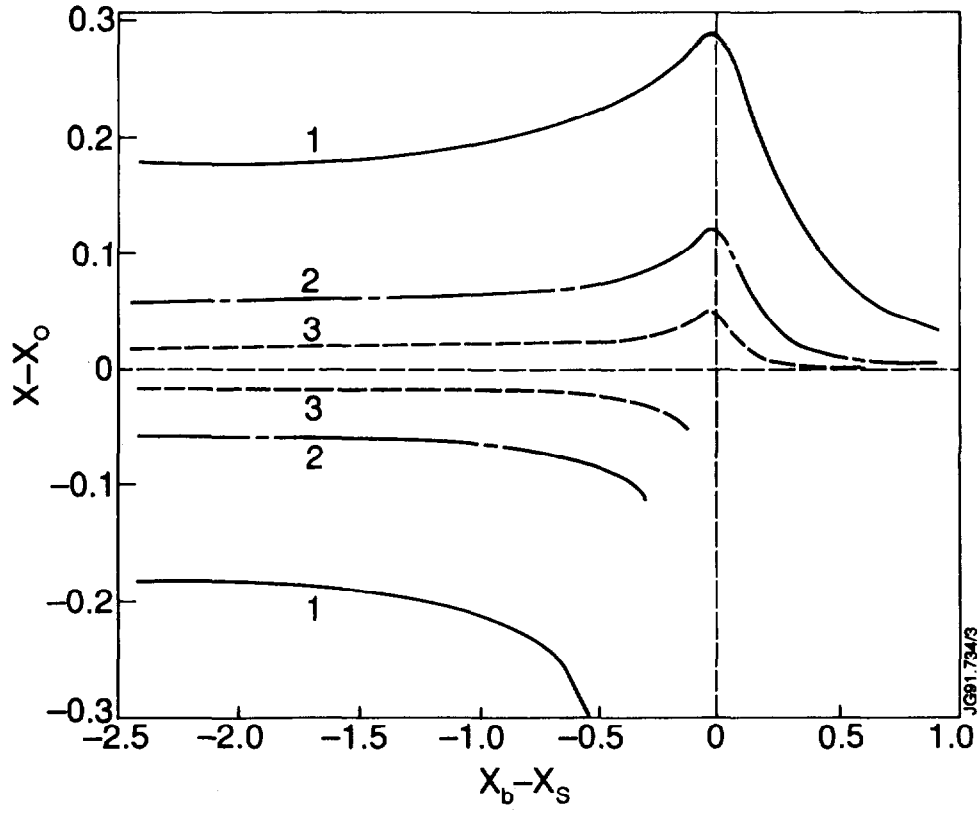


Fig. 5 x-coordinate of drift X-point ($x_d$) at the line $B_R = 0$ as a function of the banana tip position ($x_b$). $x_s$ = coordinate of magnetic X-point. 1) E = 1 MeV, 2) E = 100 keV, 3) E = 10 keV. Curves with $\Delta x < 0$ correspond to transit particles with $v_{||} < 0$; $x_o$ =

$$\begin{cases} O; & x_b < 0, \\ x_b; & x_b \geq 0. \end{cases}$$

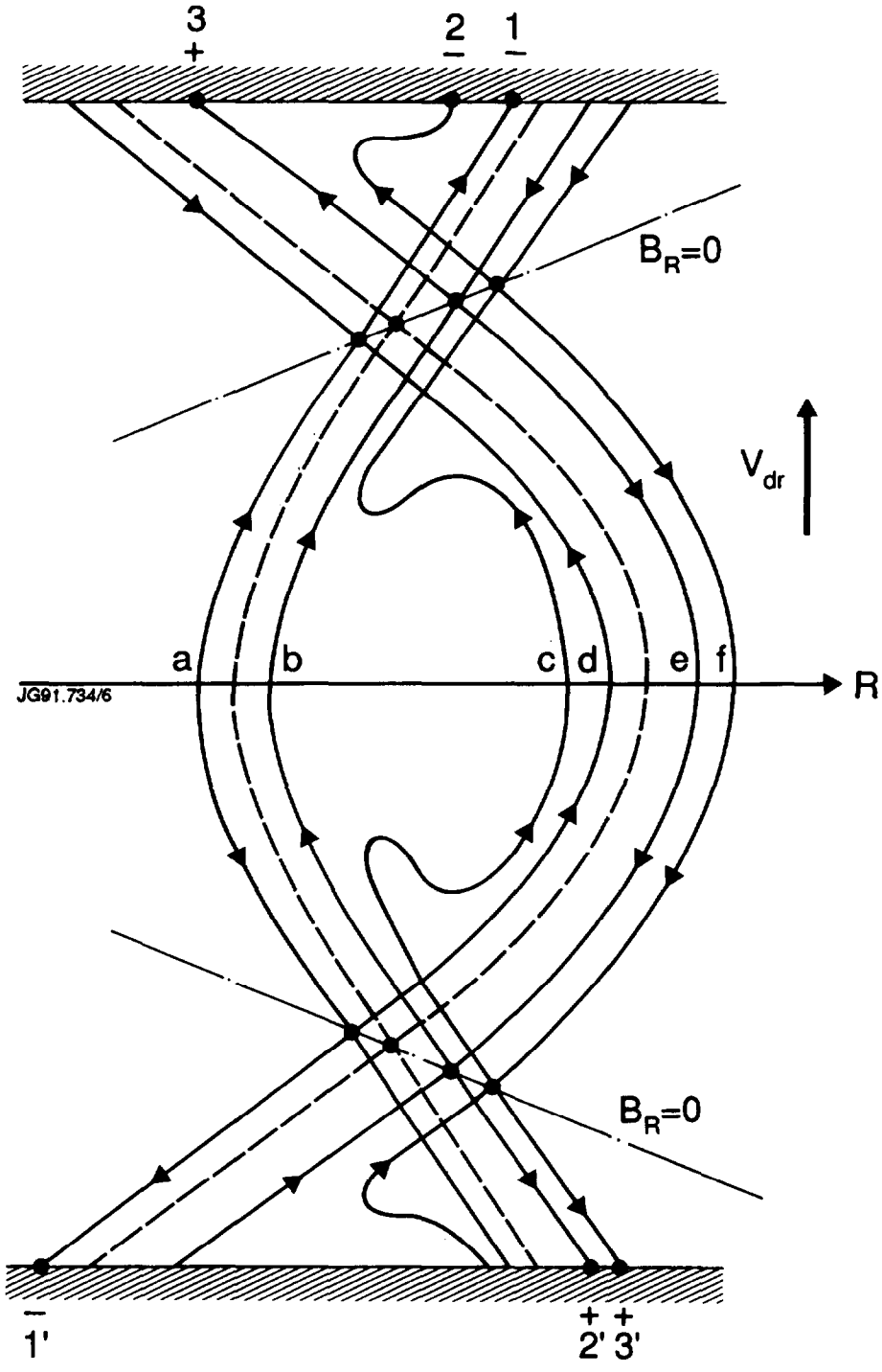


Fig. 6 Qualitative picture of separatrix drift surfaces. Signs '+' and '-' indicate the direction of particle velocity at the striking point. '+' corresponds to particles moving in the direction of plasma current, and '-' to particles moving in the opposite direction.

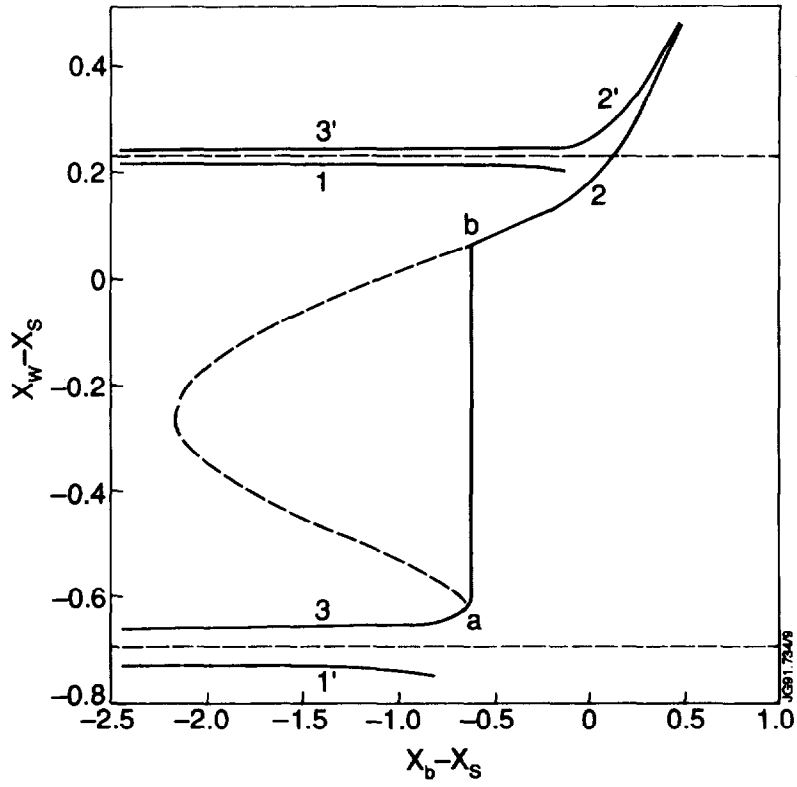


Fig. 7 The positions of drift separatrix striking points at the target plate, $x_w$, as a function of banana tip position, $x_b$, for particle energy E = 10 keV. $x_s$ = coordinate of magnetic X-point. Horizontal target plate located at the distance $z_w = 0.4$ from the magnetic X-point. Different curves correspond to different orbits shown in Fig. 6. Dashed lines show magnetic separatrix striking points positions.

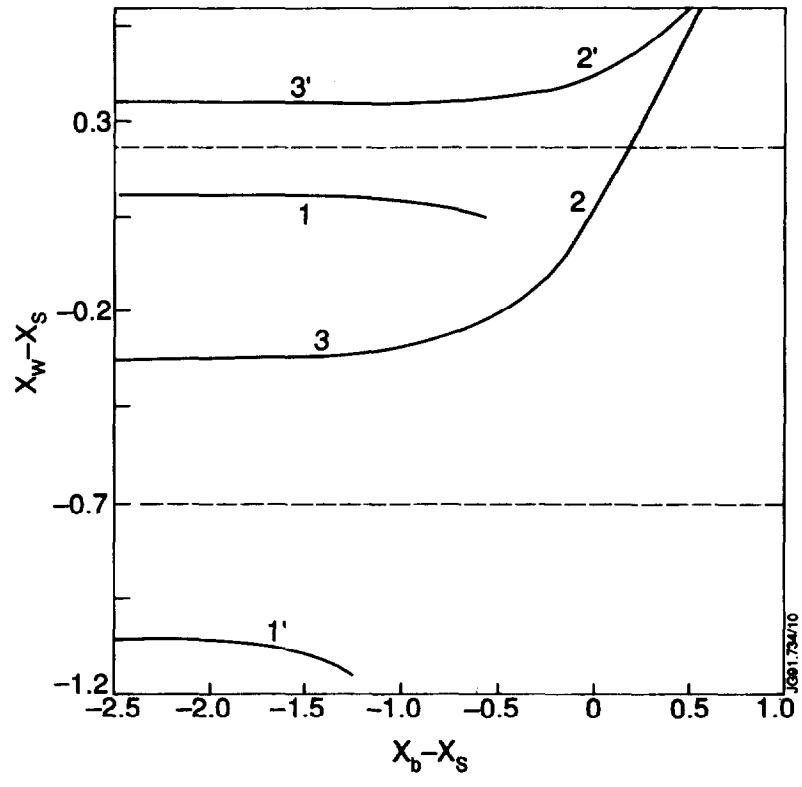


Fig. 8 The same as in Fig. 7 but for the particle energy of 1 MeV.

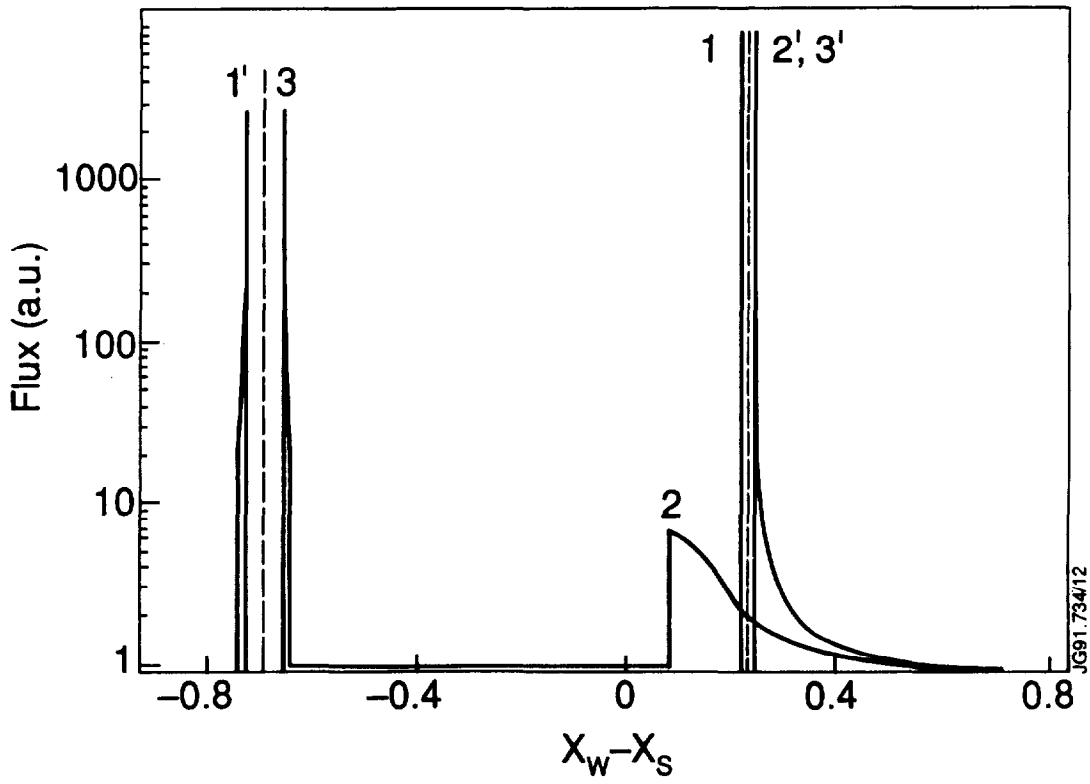


Fig. 9 The flux profile at the target plate for particles with E = 10 keV. Different peaks correspond to different orbits shown in Fig. 6. $x_s$ - coordinate of magnetic X-point.

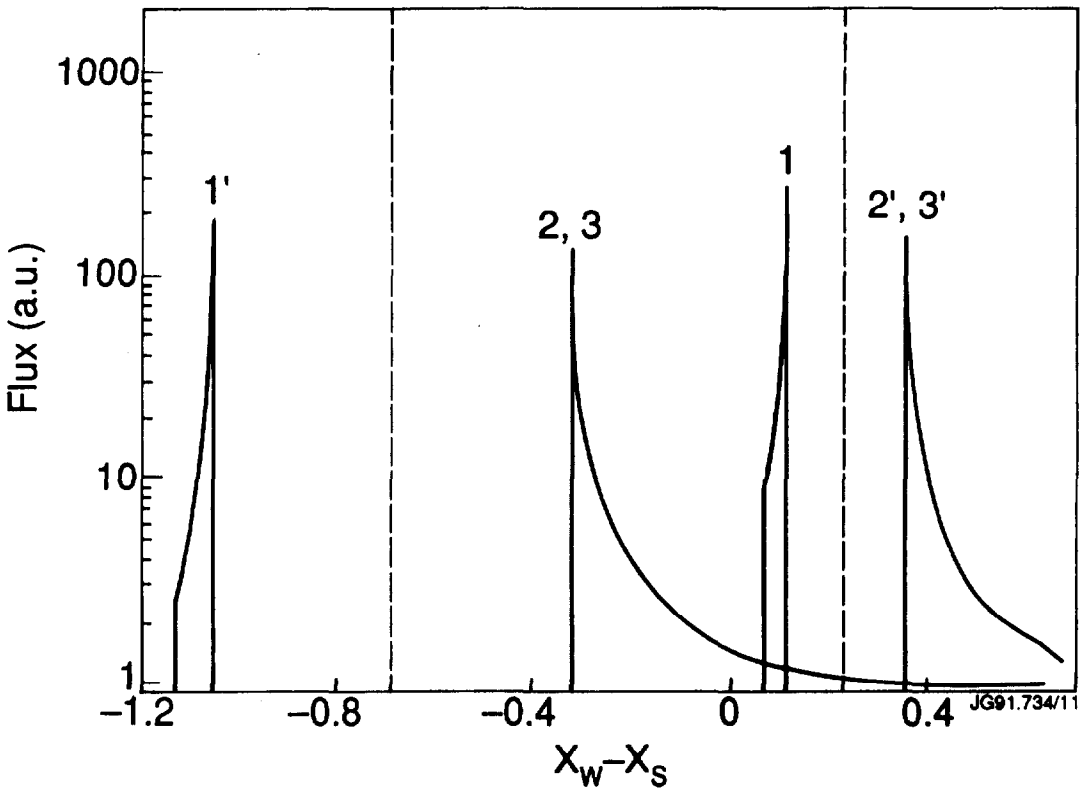


Fig. 10 The same as in Fig. 9 but for the particle energy of 1 MeV.

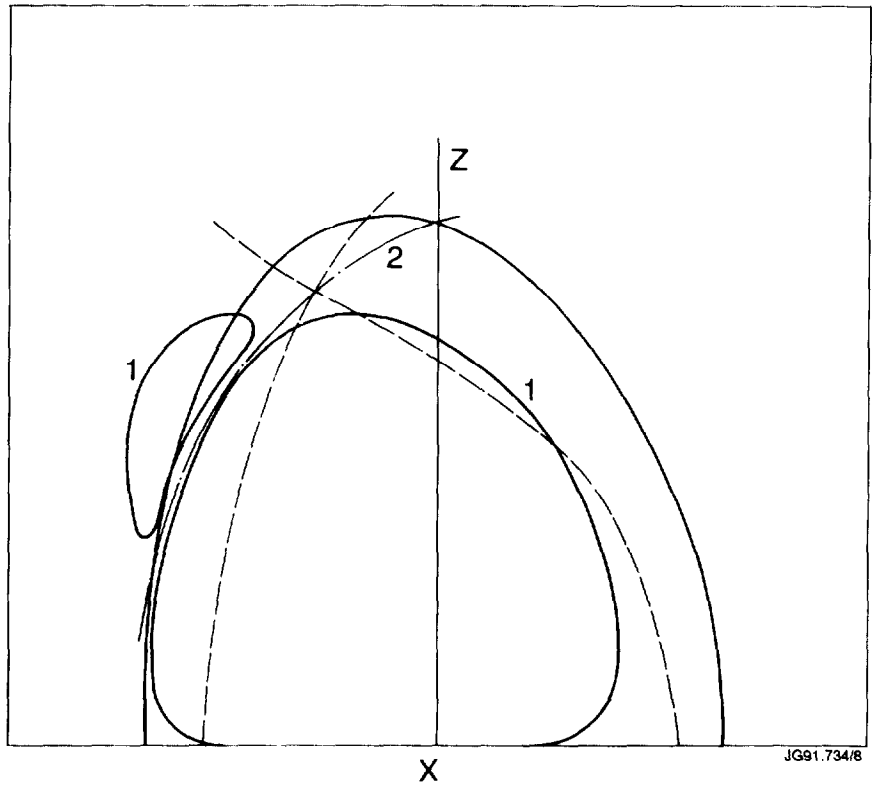


Fig. 11 Position of ripple well region boundary (1) and line $B_R = 0$ (2) in the plasma cross section.

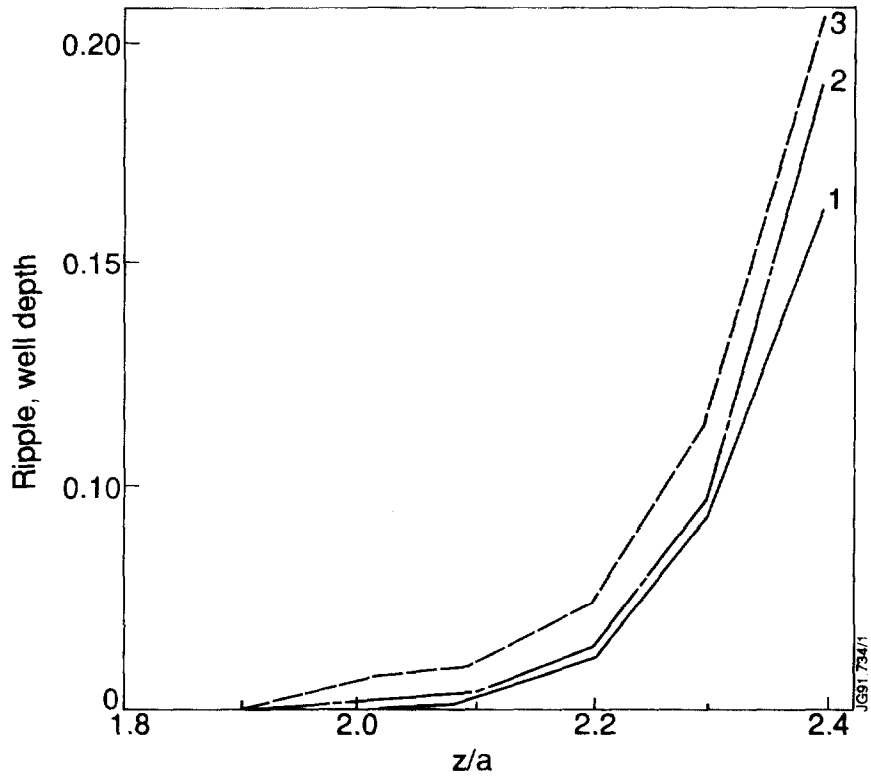


Fig. 12 Ripple well depth vs. z. 1) x = -0.75, 2) x = -0.5, 3) x = -0.25.

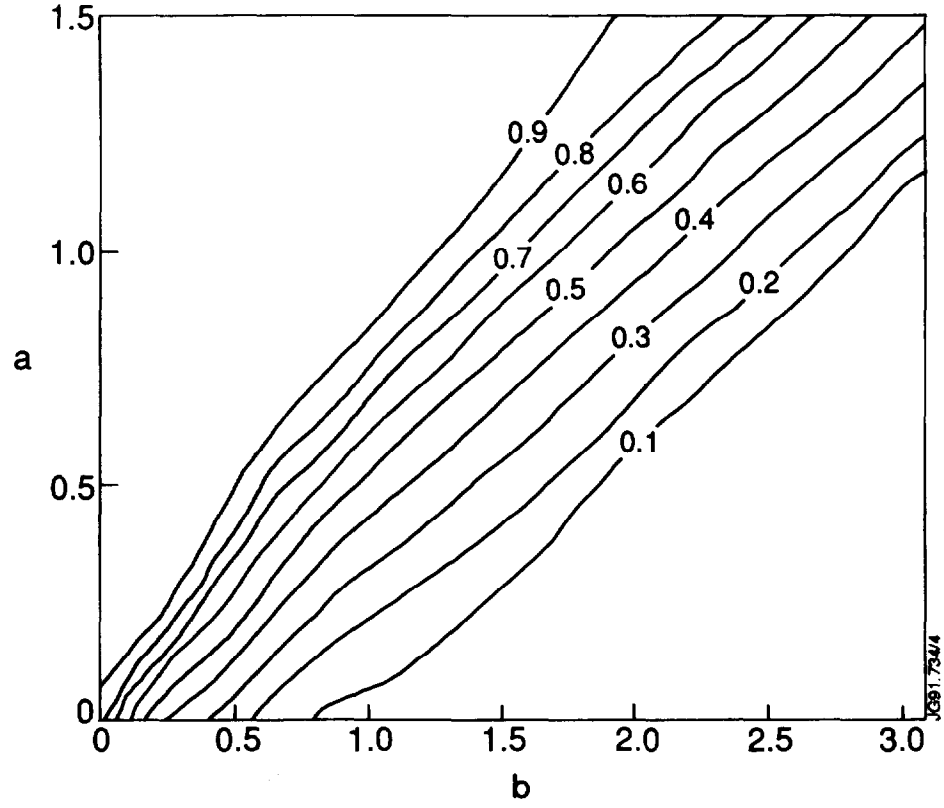


Fig. 13 Contours of the probability of ripple well trapping in the plane a,b.

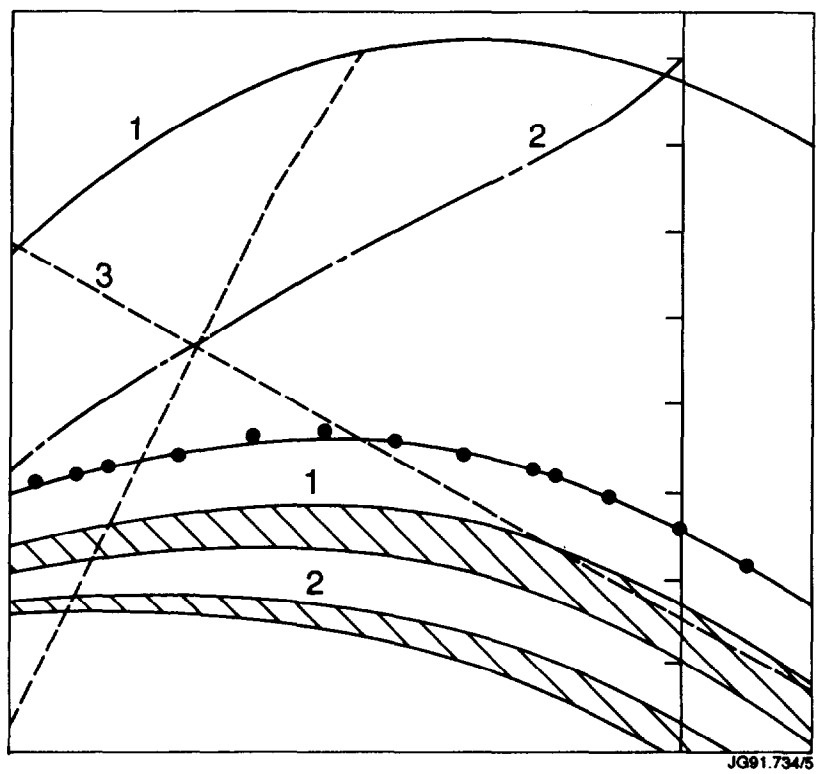


Fig. 14 Position of ripple well region boundary (curve with circles). For high energy particles probability of the trapping changes from zero to 0.8 when the banana tip position moves across shadowed regions. 1) E = 250 keV, 2) E = 1 MeV.

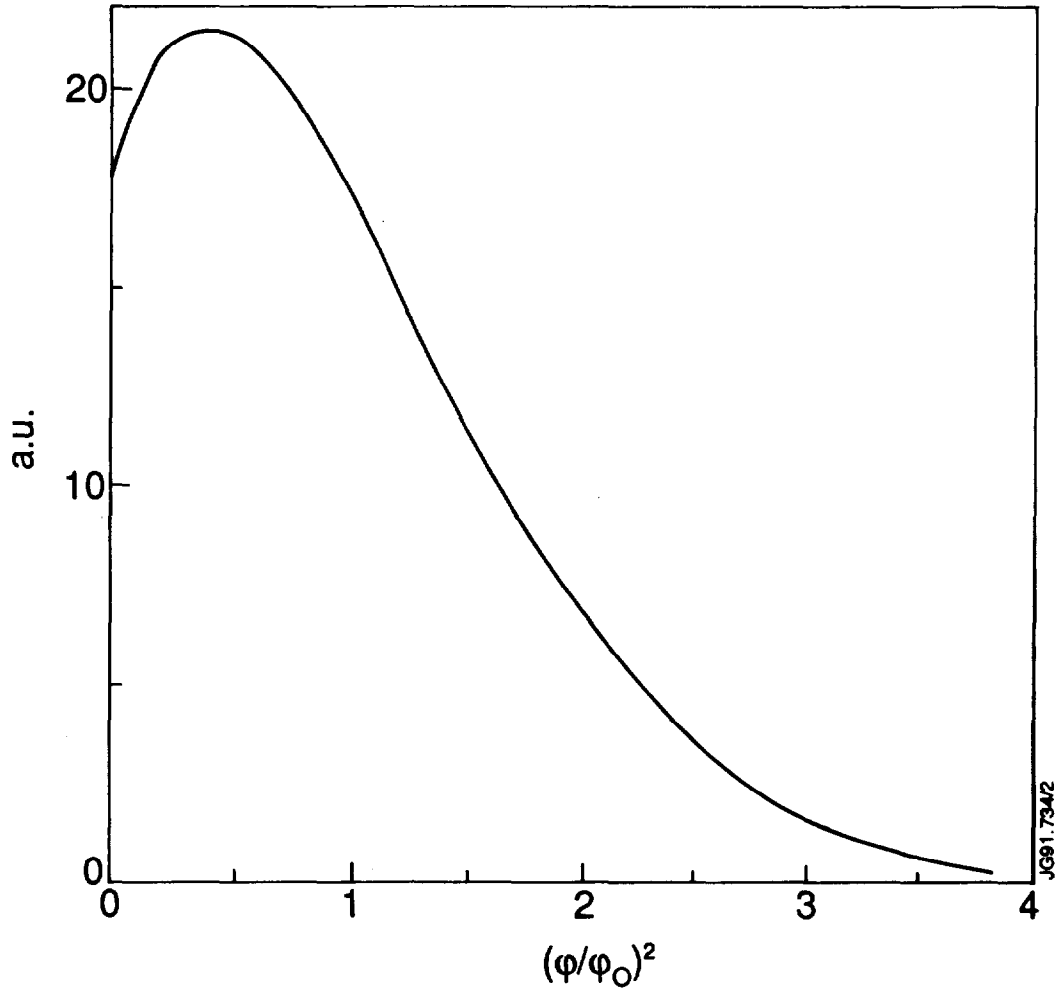


Fig. 15 Toroidal distribution of the ripple trapped particle flux.

# ANNEX

P.-H. REBUT, A. GIBSON, M. HUGUET, J.M. ADAMS[1], B. ALPER, H. ALTMANN, A. ANDERSEN[2], P. ANDREW[3], M. ANGELONE[4], S. ALI-ARSHAD, P. BAIGGER, W. BAILEY, B. BALET, P. BARABASCHI, P. BARKER, R. BARNSLEY[5], M. BARONIAN, D.V. BARTLETT, L. BAYLOR[6], A.C. BELL, G. BENALI, P. BERTOLDI, E. BERTOLINI, V. BHATNAGAR, A.J. BICKLEY, D. BINDER, H. BINDSLEV[2], T. BONICELLI, S.J. BOOTH, G. BOSIA, M. BOTMAN, D. BOUCHER, P. BOUCQUEY, P. BREGER, H. BRELEN, H. BRINKSCHULTE, D. BROOKS, A. BROWN, T. BROWN, M. BRUSATI, S. BRYAN, J. BRZOZOWSKI[7], R. BUCHSE[22], T. BUDD, M. BURES, T. BUSINARO, P. BUTCHER, H. BUTTGEREIT, C. CALDWELL-NICHOLS, D.J. CAMPBELL, P. CARD, G. CELENTANO, C.D. CHALLIS, A.V. CHANKIN[8], A. CHERUBINI, D. CHIRON, J. CHRISTIANSEN, P. CHUILON, R. CLAESEN, S. CLEMENT, E. CLIPSHAM, J.P. COAD, I.H. COFFEY[9], A. COLTON, M. COMISKEY[10], S. CONROY, M. COOKE, D. COOPER, S. COOPER, J.G. CORDEY, W. CORE, G. CORRIGAN, S. CORTI, A.E. COSTLEY, G. COTTRELL, M. COX[11], P. CRIPWELL[12], O. Da COSTA, J. DAVIES, N. DAVIES, H. de BLANK, H. de ESCH, L. de KOCK, E. DEKSNIS, F. DELVART, G.B. DENNE-HINNOV, G. DESCHAMPS, W.J. DICKSON[13], K.J. DIETZ, S.L. DMITRENKO, M. DMITRIEVA[14], J. DOBBING, A. DOGLIO, N. DOLGETTA, S.E. DORLING. P.G. DOYLE, D.F. DÜCHS, H. DUQUENOY, A. EDWARDS, J. EHRENBERG, A. EKEDAHL, T. ELEVANT[7], S.K. ERENTS[11], L.G. ERIKSSON, H. FAJEMIROKUN[12], H. FALTER, J. FREILING[15], F. FREVILLE, C. FROGER, P. FROISSARD, K. FULLARD, M. GADEBERG, A. GALETSAS, T. GALLAGHER, D. GAMBIER, M. GARRIBBA, P. GAZE, R. GIANNELLA, R.D. GILL, A GIRARD, A. GONDHALEKAR, D. GOODALL[11], C. GORMEZANO, N.A. GOTTARDI, C. GOWERS, B.J. GREEN, B. GRIEVSON, R. HAANGE, A. HAIGH, C.J. HANCOCK, P.J. HARBOUR, T. HARTRAMPF, N.C. HAWKES[11], P. HAYNES[11], J.L. HEMMERICH, T. HENDER[11], J. HOEKZEMA, D. HOLLAND, M. HONE, L. HORTON, J. HOW, M. HUART, I. HUGHES, T.P. HUGHES[10], M. HUGON, Y. HUO[16], K. IDA[17], B. INGRAM, M. IRVING, J. JACQUINOT, H. JAECKEL, J.F. JAEGER, G. JANESCHITZ, Z. JANKOVICZ[18], O.N. JARVIS, F. JENSEN, E.M. JONES, H.D. JONES, L.P.D.F. JONES, S. JONES[19], T.T.C. JONES, J.-F. JUNGER, F. JUNIQUE, A. KAYE, B.E. KEEN, M. KEILHACKER, G.J. KELLY, W. KERNER, A. KHUDOLEEV[21], R. KONIG, A. KONSTANTELLOS, M. KOVANEN[20], G. KRAMER[15], P. KUPSCHUS, R. LÄSSER, J.R. LAST, B. LAUNDY, L. LAURO-TARONI, M. LAVEYRY, K. LAWSON[11], M. LENNHOLM, J. LINGERTAT[22], R.N. LITUNOVSKI, A. LOARTE, R. LOBEL, P. LOMAS, M. LOUGHLIN, C. LOWRY, J. LUPO, A.C. MAAS[15], J. MACHUZAK[19], B. MACKLIN, G. MADDISON[11], C.F. MAGGI[23], G. MAGYAR, W. MANDL[22], V. MARCHESE, G. MARCON, F. MARCUS, J. MART, D. MARTIN, E. MARTIN, R. MARTIN-SOLIS[24], P. MASSMANN, G. MATTHEWS, H. McBRYAN, G. McCRACKEN[11], J. McKIVITT, P. MERIGUET, P. MIELE, A. MILLER, J. MILLS, S.F. MILLS, P. MILLWARD, P. MILVERTON, E. MINARDI[4], R. MOHANTI[25], P.L. MONDINO, D. MONTGOMERY[26], A. MONTVAI[27], P. MORGAN, H. MORSI, D. MUIR, G. MURPHY, R. MYRNÄS[28], F. NAVE[29], G. NEWBERT, M. NEWMAN, P. NIELSEN, P. NOLL, W. OBERT, D. O'BRIEN, J. ORCHARD, J. O'ROURKE, R. OSTROM, M. OTTAVIANI, M. PAIN, F. PAOLETTI, S. PAPASTERGIOU, W. PARSONS, D. PASINI, D. PATEL, A. PEACOCK, N. PEACOCK[11], R.J.M. PEARCE, D. PEARSON[12], J.F. PENG[16], R. PEPE DE SILVA, G. PERINIC, C. PERRY, M. PETROV[21], M.A. PICK, J. PLANCOULAINE, J.-P POFFÉ, R. PÖHLCHEN, F. PORCELLI, L. PORTE[13], R. PRENTICE, S. PUPPIN, S. PUTVINSKII[8], G. RADFORD[30], T. RAIMONDI, M.C. RAMOS DE ANDRADE, R. REICHLE, J. REID, S. RICHARDS, E. RIGHI, F. RIMINI, D. ROBINSON[11], A. ROLFE, R.T. ROSS, L. ROSSI, R. RUSS, P. RUTTER, H.C. SACK, G. SADLER, G. SAIBENE, J.L. SALANAVE, G. SANAZZARO, A. SANTAGIUSTINA, R. SARTORI, C. SBORCHIA, P. SCHILD, M. SCHMID, G. SCHMIDT[31], B. SCHUNKE, S.M. SCOTT, L. SERIO, A SIBLEY, R. SIMONINI, A.C.C. SIPS, P. SMEULDERS, R. SMITH, R. STAGG, M. STAMP, P. STANGEBY[3], R. STANKIEWICZ[32], D.F. START, C.A. STEED, D. STORK, P.E. STOTT, P. STUBBERFIELD, D. SUMMERS, H. SUMMERS[13], L. SVENSSON, J.A. TAGLE[33], M. TALBOT, A. TANGA, A. TARONI, C. TERELLA, A TERRINGTON, A TESINI, P.R. THOMAS, E. THOMPSON, K. THOMSEN, F. TIBONE, A. TISCORNIA, P. TREVALION, B. TUBBING, P. VAN BELLE, H. VAN DER BEKEN, G. VLASES, M. VON HELLERMANN, T. WADE, C. WALKER, R. WALTON[31], D. WARD, M.L. WATKINS, N. WATKINS, M.J. WATSON, S. WEBER[34], J. WESSON, T.J. WIJNANDS, J. WILKS, D. WILSON, T. WINKEL, R. WOLF, D. WONG, C. WOODWARD, Y. WU[35], M. WYKES, D. YOUNG, I.D. YOUNG, L. ZANNELLI, A. ZOLFAGHARI[19], W. ZWINGMANN

[1] Harwell Laboratory, UKAEA, Harwell, Didcot, Oxfordshire, UK.
[2] Risø National Laboratory, Roskilde, Denmark.
[3] Institute for Aerospace Studies, University of Toronto, Downsview, Ontario, Canada.
[4] ENEA Frascati Energy Research Centre, Frascati, Rome, Italy.
[5] University of Leicester, Leicester, UK.
[6] Oak Ridge National Laboratory, Oak Ridge, TN, USA.
[7] Royal Institute of Technology, Stockholm, Sweden.
[8] I.V. Kurchatov Institute of Atomic Energy, Moscow, Russian Federation.
[9] Queens University, Belfast, UK.
[10] University of Essex, Colchester, UK.
[11] Culham Laboratory, UKAEA, Abingdon, Oxfordshire, UK.
[12] Imperial College of Science, Technology and Medicine, University of London, London, UK.
[13] University of Strathclyde, Glasgow, UK.
[14] Keldysh Institute of Applied Mathematics, Moscow, Russian Federation.
[15] FOM-Institute for Plasma Physics "Rijnhuizen", Nieuwegein, Netherlands.
[16] Institute of Plasma Physics, Academia Sinica, Hefei, Anhui Province, China.
[17] National Institute for Fusion Science, Nagoya, Japan.
[18] Soltan Institute for Nuclear Studies, Otwock/Świerk, Poland.
[19] Plasma Fusion Center, Massachusetts Institute of Technology, Boston, MA, USA.
[20] Nuclear Engineering Laboratory, Lappeenranta University, Finland.
[21] A.F. Ioffe Physico-Technical Institute, St. Petersburg, Russian Federation.
[22] Max-Planck-Institut für Plasmaphysik, Garching, Germany.
[23] Department of Physics, University of Milan, Milan, Italy.
[24] Universidad Complutense de Madrid, Madrid, Spain.
[25] North Carolina State University, Raleigh, NC, USA.
[26] Dartmouth College, Hanover, NH, USA.
[27] Central Research Institute for Physics, Budapest, Hungary.
[28] University of Lund, Lund, Sweden.
[29] Laboratorio Nacional de Engenharia e Tecnologia Industrial, Sacavem, Portugal.
[30] Institute of Mathematics, University of Oxford, Oxford, UK.
[31] Princeton Plasma Physics Laboratory, Princeton University, Princeton, NJ, USA.
[32] RCC Cyfronet, Otwock/Świerk, Poland,
[33] Centro de Investigaciones Energéticas, Medioambientales y Tecnológicas, Madrid, Spain.
[34] Freie Universität, Berlin, Germany.
[35] Insitute for Mechanics, Academia Sinica, Beijing, China.